

Gravitational Lensing of stars in the central arcsecond of our Galaxy

V. Bozza^{1,2,3} and L. Mancini^{2,3}

¹*Centro Studi e Ricerche “Enrico Fermi”, via Panisperna 89/A, Roma, Italy.*

²*Dipartimento di Fisica “E.R. Caianiello”, Università di Salerno, via S. Allende, Baronissi (SA), Italy.*

³*Istituto Nazionale di Fisica Nucleare, Sezione di Napoli, Italy.*

ABSTRACT

In the neighborhood of Sgr A*, several stars (S2, S12, S14, S1, S8, S13) enjoy an accurate determination of their orbital parameters. General Relativity predicts that the central black hole acts as a gravitational lens on these stars, generating a secondary image and two infinite series of relativistic images. For each of these six stars, we calculate the light curves for the secondary and the first two relativistic images, in the Schwarzschild black hole hypothesis, throughout their orbital periods. The curves are peaked around the periaapse epoch, but two subpeaks may arise in nearly edge-on orbits, when the source is behind or in front of Sgr A*. We show that for most of these stars the secondary image should be observable during its brightness peak. In particular, S14 is the best candidate, since its secondary image reaches $K=23.3$ with an angular separation of 0.125 mas from the apparent horizon of the central black hole. The detection of such images by future instruments could represent the first observation of gravitational lensing beyond the weak field approximation.

Subject headings: Gravitational lensing — Black hole physics — Stars: individual(S2,S12,S14,S1,S8,S13) — Galaxy: center

1. Introduction

In the last years, the existence of a supermassive black hole corresponding to the radio source Sgr A* has been established on a quite solid ground (Melia & Falcke 2001). The studies of stellar dynamics in the neighborhood of Sgr A* have played a major role in this scientific process providing strong evidence in favor of the existence of a huge point-like mass

hidden in this radio source. The most accurate observations have been led by an American group at Keck (Ghez et al. 1998, 2003, 2005), and by a German group at VLT (Eckart & Genzel 1997; Genzel et al. 1996; Eckart et al. 2002; Schödel et al. 2002, 2003; Eisenhauer et al. 2005).

The measurement of the proper motions of stars very close to the central black hole has led to a three-dimensional reconstruction of the orbits of six stars, named S2, S12, S14, S1, S8, S13 by Schödel et al. (2003) and S0-2, S0-19, S0-16, S0-1, S0-4, S0-20 by Ghez et al. (2005), respectively. The ambiguity on the sign of the inclination was resolved for the first of these stars by Doppler shift measures (Ghez et al. 2003). Then, very recently, further measurements have resolved this ambiguity also for the remaining stars (Eisenhauer et al. 2005). Now the orbital parameters of all of them are known to an accuracy reasonable enough to start investigations relying on the knowledge of the geometric configurations between the star and the central black hole. Indeed one of the most interesting effects to search for is gravitational lensing.

The bending of light by gravitational fields is an invaluable instrument to investigate the properties of the lensing object, its mass distribution, the gravitational potential and many general relativistic effects. The stars around the black hole at the Galactic Center provide a unique lab for gravitational lensing researches, which may have very much to say in the near future on gravitational physics.

The first studies of gravitational lensing by Sgr A* have been performed by Wardle & Yusuf-Zadeh (1992), who focused on sources in the stellar cluster surrounding it. They realized that gravitational lensing would slightly deplete the sky of visible stars in a region of radius 10 mas, pushing them to 30 mas. However, such a statistical effect is practically unobservable given the observed stellar density in the neighborhood of Sgr A*. Gravitational lensing could be recognized by identifying opposite images of a star passing behind the central black hole. Several stars should be significantly lensed at a given time. Estimates by Jaroszyński (1998), Alexander & Sternberg (1999), Chanamé et al. (2001) agree that roughly 10 stars in the Galactic bulge are simultaneously lensed by Sgr A* with a detection threshold for the secondary image of 23 mag in the K-band. However, recognizing gravitational lensed images is by no way a trivial task. While the secondary image would stay very close to the central black hole (at about 30 mas), the direct image of the source could be displaced by as much as several arcsecs. The association between the two images could be established on the basis of common spectral properties, flux variation and full correlation in their proper motions (the lensing event should have a duration of some months). Eventual observations of several pairs of images could pinpoint the exact position of the black hole (Alexander 2001). The secondary images could be additionally lensed by a possible population of stellar

size black holes around the supermassive one (Alexander & Loeb 2001; Chanamé et al. 2001; Munro et al. 2004), though such a double microlensing event is relatively unlikely. Another possibility is to measure the shift of the apparent position of a star passing just behind the black hole (Nusser & Broadhurst 2004). Such a measurement, would provide an independent estimate of the distance of Sgr A*.

Coming to our six stars, we have an evident advantage: we precisely know their location in space as a function of time and thus the geometry of the lensing configuration. Since we already observe the direct image, we can predict at any time where to look for a secondary lensing image and what its apparent magnitude should be. Thanks to our knowledge of their orbits, we can easily predict the best time to observe these secondary images. Finally, since the distances between the sources and the lens are known, the information extraction from gravitational lensing observations is much easier and unambiguous.

A very important fact that must be taken into account in the study of the light curves of gravitational lensing images is that the weak field regime for the secondary image holds only for a very good alignment between source, lens and observer. This is not the case for the six stars studied in this article. This forces us to resort to the full General Relativity deflection angle formula, which is very well known since old times in terms of elliptic integrals (Darwin 1959). The deflection angle diverges logarithmically at a characteristic minimum impact angle for any class of spherically symmetric black holes (Bozza 2002), implying the existence of two infinite series of "ghosts", as called by Darwin (1959), or relativistic images, as named by Virbhadra & Ellis (2000). These images are due to photons winding one or more times around the black holes and are usually extremely faint. Moreover, they would appear very close to the central black hole, at angular separations comparable to the apparent Schwarzschild horizon, which is about $23 \mu\text{as}$. The detection of such images would thus require a higher order technological effort, including very long baseline interferometry in the K-band and very high sensitivity. However, these images are very precious witnesses of the extreme gravitational field at distances slightly larger than the Schwarzschild radius of the central black hole. The information stored in them is of striking importance to unveil the features of the true gravitational theory and the mysteries on the physics of the central black hole. Relativistic images produced by Sgr A* have also been studied by Petters (2003), who noticed that their contribution to microlensing is negligible, and by Eiroa & Torres (2004) in the context of retro-lensing.

S2 was the first star around Sgr A* to be studied as a possible source for gravitational lensing effects (De Paolis et al. 2003). Even if its orbit never allows a good alignment with Sgr A*, the secondary image can reach $K \lesssim 30$ while it is in a fully relativistic regime. In a previous work (Bozza & Mancini 2004), we presented a complete study of S2 gravitational

lensing using the tools of the Strong Field Limit method (Bozza et al. 2001; Bozza 2002). In this way we have been able to predict the precise epoch of the best observability of the secondary image.

In this paper we develop a complete analysis of the six aforementioned stars as potential sources for gravitational lensing by the central black hole, finding interesting results, especially for the star S14. To cover the whole range of gravitational lensing regimes, from strong to weak, we will exclusively use the exact deflection formula known for the Schwarzschild black hole. In this way we can achieve a very reliable and precise description for the light curves of all images.

Our paper is structured as follows. In § 2 we review the exact Schwarzschild deflection formula and some basics of gravitational lensing. In § 3 we recall the features of the six stars we want to examine, discussing the geometry of their orbits. In § 4 we present the results of our analysis, with the light curves of our six stars and the positions of the secondary images. In § 5 we discuss the perspectives for observations of these images using long baseline interferometry. Finally, § 6 contains the conclusions.

2. Schwarzschild gravitational lensing

Consider the generic three-point configuration between source, lens and observer, illustrated in Figure 1. We indicate by D_{OL} , D_{LS} and D_{OS} the distance between observer and lens, lens and source, observer and source respectively. All the distances are measured in terms of the Schwarzschild radius of the black hole

$$R_{Sch} = \frac{2GM}{c^2}. \quad (1)$$

We call optical axis the line connecting the observer and the lens. We denote by γ the angle between the line connecting the source to the lens and the optical axis, and by β the angle formed by the line connecting source and observer with the optical axis. The direct image of the source suffers (weak) gravitational lensing only when γ is very close to zero. The secondary image is formed by photons passing behind the black hole, as shown in Figure 1. The impact angles for the photons as seen from the observer and the source are θ and $\bar{\theta}$, respectively. The deflection angle is defined as the angle between the asymptotic directions of motion of the photons, before and after the encounter with the black hole.

By inspection of Figure 1, we can write down the following lens equation

$$\gamma = \alpha(\theta) - \theta - \bar{\theta}. \quad (2)$$

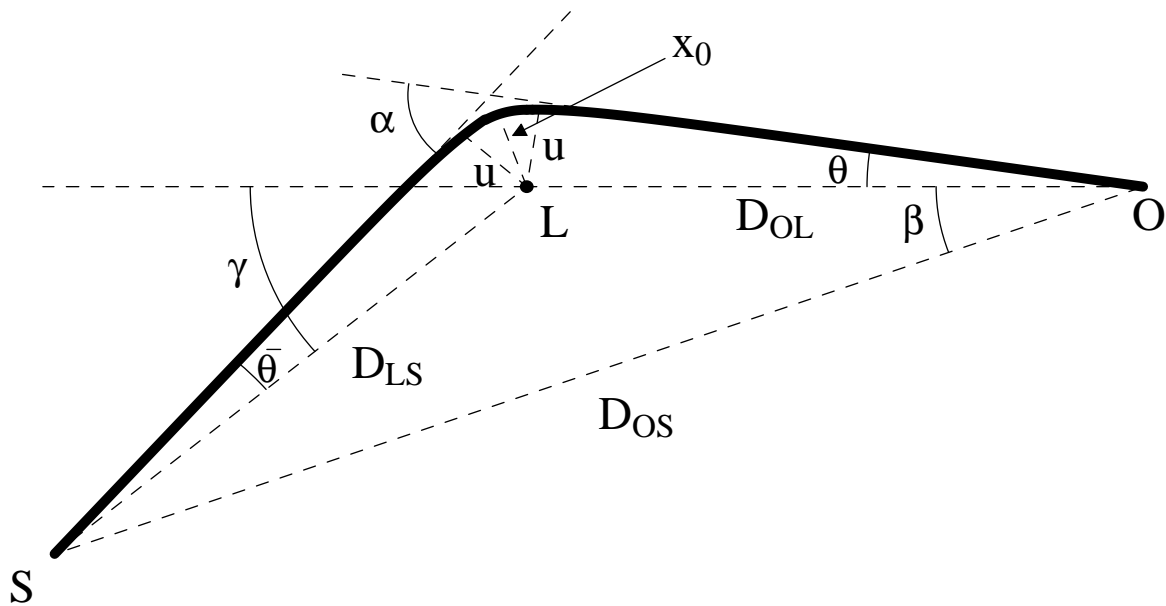


Fig. 1.— A generic lensing configuration.

The impact parameter u is related to the impact angles θ and $\bar{\theta}$ by

$$u = D_{OL} \sin \theta = D_{LS} \sin \bar{\theta}. \quad (3)$$

This relation can be used to eliminate $\bar{\theta}$ in favor of θ . The position angle of the source γ runs from 0 (perfect alignment) to π (perfect anti-alignment).

Besides the direct and the secondary image, we also have higher order relativistic images, which form closer to the central black hole. Because of their potential importance as probes of very strong gravitational fields, in our analysis we will also discuss the third and the fourth order image. The third order image is formed by photons turning around the black hole and reaching the observer from the same side of the direct image. It is described by a lens equation of the type

$$2\pi - \gamma = \alpha(\theta) - \theta - \bar{\theta}. \quad (4)$$

Notice that the deflection angle $\alpha(\theta)$ is in the range $[\pi, 2\pi]$.

The fourth order image is formed by photons performing a complete loop around the black hole and reaching the observer from the side of the secondary image. It is described by a lens equation of the type

$$2\pi + \gamma = \alpha(\theta) - \theta - \bar{\theta}. \quad (5)$$

The required deflection angle is in the range $[2\pi, 3\pi]$.

The direct and the third order image have positive parity while the secondary and the fourth order ones have negative parity.

The exact deflection angle was calculated by Darwin (1959) in terms of elliptic integrals. It can be written as a function of the closest approach distance x_0 as

$$\alpha(x_0) = -\pi - 4F(\varphi_0, \lambda) G(x_0), \quad (6)$$

where

$$G(x_0) = \sqrt{\frac{8x_0 \left(-3 + x_0 + \sqrt{(-1 + x_0)(3 + x_0)} \right)}{3 - 2x_0}} \quad (7)$$

and

$$F(\varphi_0, \lambda) = \int_0^{\varphi_0} (1 - \lambda \sin^2 \varphi)^{-1/2} d\varphi \quad (8)$$

is an elliptic integral of first kind. The parameters φ_0 and λ are themselves functions of x_0 :

$$\varphi_0 = \arcsin \sqrt{\frac{-3 + x_0 - \sqrt{-3 + 2x_0 + x_0^2}}{2(-3 + 2x_0)}}, \quad (9)$$

and

$$\lambda = \frac{3 - x_0 - \sqrt{-3 + 2x_0 + x_0^2}}{3 - x_0 + \sqrt{-3 + 2x_0 + x_0^2}}. \quad (10)$$

The relation between the closest approach distance x_0 and the impact parameter u can be easily found by the conservation of angular momentum

$$x_0^2 = \left(1 - \frac{1}{x_0}\right) u^2. \quad (11)$$

The use of the exact formula (6) is rather cumbersome in analytical applications. Actually, before Darwin's work only the weak field limit for large impact parameters was known. In Schwarzschild units, it reads

$$\alpha_{WFL} = \frac{2}{u}. \quad (12)$$

The opposite limit is recovered when u approaches its minimum value $u_m = 3\sqrt{3}/2$. In this limit, we have (Darwin 1959; Ohanian 1987; Bozza et al. 2001)

$$\alpha_{SFL} = -\log\left(\frac{u}{u_m} - 1\right) + \log\left[216(7 - 4\sqrt{3})\right] - \pi. \quad (13)$$

This formula was later extended by Bozza (2002) to a generic spherically symmetric black hole and to a Kerr black hole for equatorial motion (Bozza 2003). The logarithmic divergence of the deflection angle at the minimum impact parameter signals the presence of an infinite sequence of images with deflection angles which differ by a multiple of 2π (an arbitrary number of loops around the black hole). For impact parameters below u_m , the photon is always captured by the black hole. The striking importance of higher order images comes from the fact that they can be directly related to the values of the metric components and their derivatives close to the horizon (Bozza 2002). This provides a unique way to identify the class to which the black hole belongs, possibly giving hints on the correct gravitational theory that holds in the strong field regime.

In Figure 2, we compare the exact deflection angle with the two approximations. We see that the weak field limit is valid only for very small deflection angles at large impact parameters, while the strong field limit starts to be accurate from $\alpha = \pi$ at impact parameters very close to the minimum value. For our purpose neither of the two limits is suitable, since the secondary image demands a deflection angle in the whole range $[0, \pi]$.

Our strategy is to solve the exact lens equations for the direct, the secondary, the third order and fourth order image, using the approximate solutions as starting points (the weak field solution for the direct and the strong field ones for the others). We shall keep the

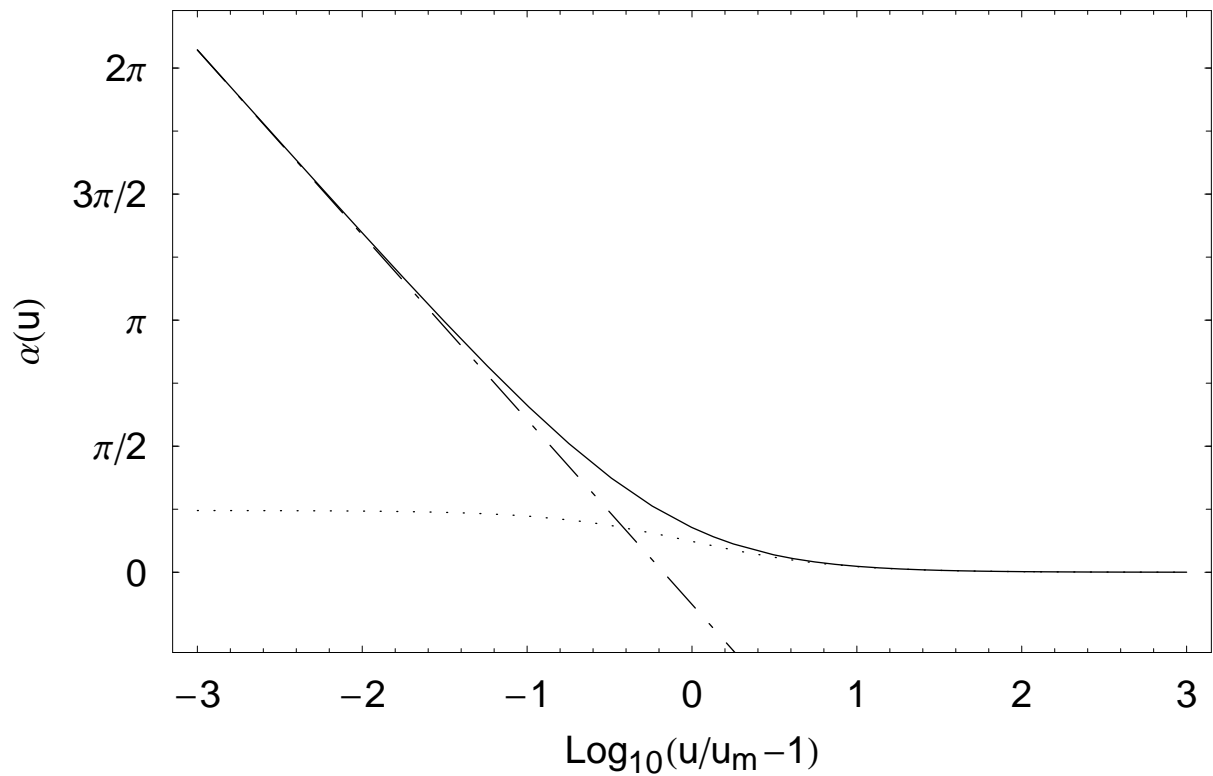


Fig. 2.— Comparison between the exact deflection angle (solid line), the weak field approximation (dotted line) and the strong field limit approximation (dot-dashed line), as functions of $\text{Log}_{10}(u/u_m - 1)$.

terms θ and $\bar{\theta}$ in the equations, since they are relevant in the weak field regime and in the intermediate one, though they become very small in the strong field regime, at least for the sources considered here.

The magnification of an image at angle θ is given by the general formula

$$\mu = \frac{D_{OS}^2}{D_{LS}^2} \frac{\sin \theta}{\frac{d\gamma}{d\theta} \sin \gamma}. \quad (14)$$

The derivative can be suitably approximated by the finite difference ratio, as we do not solve the lens equation analytically. Armed with these tools, once we know the absolute magnitude and the position of a star around Sgr A*, we can give the position and the apparent magnitude of its four most relevant images.

3. Gravitational Lensing candidates around Sgr A*

In the neighborhood of Sgr A*, proper motion and Doppler measurements have strongly increased our knowledge of stellar dynamics in this region. For six stars a complete reconstruction of the orbit has been achieved (Fig. 3). For our analysis we shall follow the latest data published by Eisenhauer et al. (2005). Alternative solutions (compatible within uncertainties) for the orbits of these six stars, derived by different measurements and methodologies, can be found in Ghez et al. (2005).

All these stars appear to belong to early spectral types B0-B9 (Eisenhauer et al. 2005), opening questions about the presence of such young stars in the inner few hundredths of a parsec around the Galactic center. Table 1 sums up their orbital parameters, taken from Eisenhauer et al. (2005). These stars have been observed in the K-band centered on $\lambda = 2.2 \mu\text{m}$, in which the extinction has been estimated to be 2.8 mag (Eisenhauer et al. 2005). In these new data all the uncertainties have been drastically reduced, save for S13, whose orbital plane is still largely undetermined. In our analysis, we will only use the best fit values of each parameter. In the last section we will discuss how the uncertainties may affect our predictions. The Schwarzschild radius of the central black hole is

$$R_{Sch} = \frac{2GM_{BH}}{c^2} = 0.071 \text{ AU}, \quad (15)$$

taking for its mass the value $M_{BH} = 3.61 \times 10^6 M_{\odot}$ (Eisenhauer et al. 2005). The distance of the Sun from the Galactic center is currently estimated to $D_{OL} \simeq 8 \text{ kpc}$ (Reid 1993); then the apparent size of the event horizon is

$$\theta_m = \frac{3\sqrt{3}R_{Sch}}{2D_{OL}} = 23\mu\text{as}. \quad (16)$$

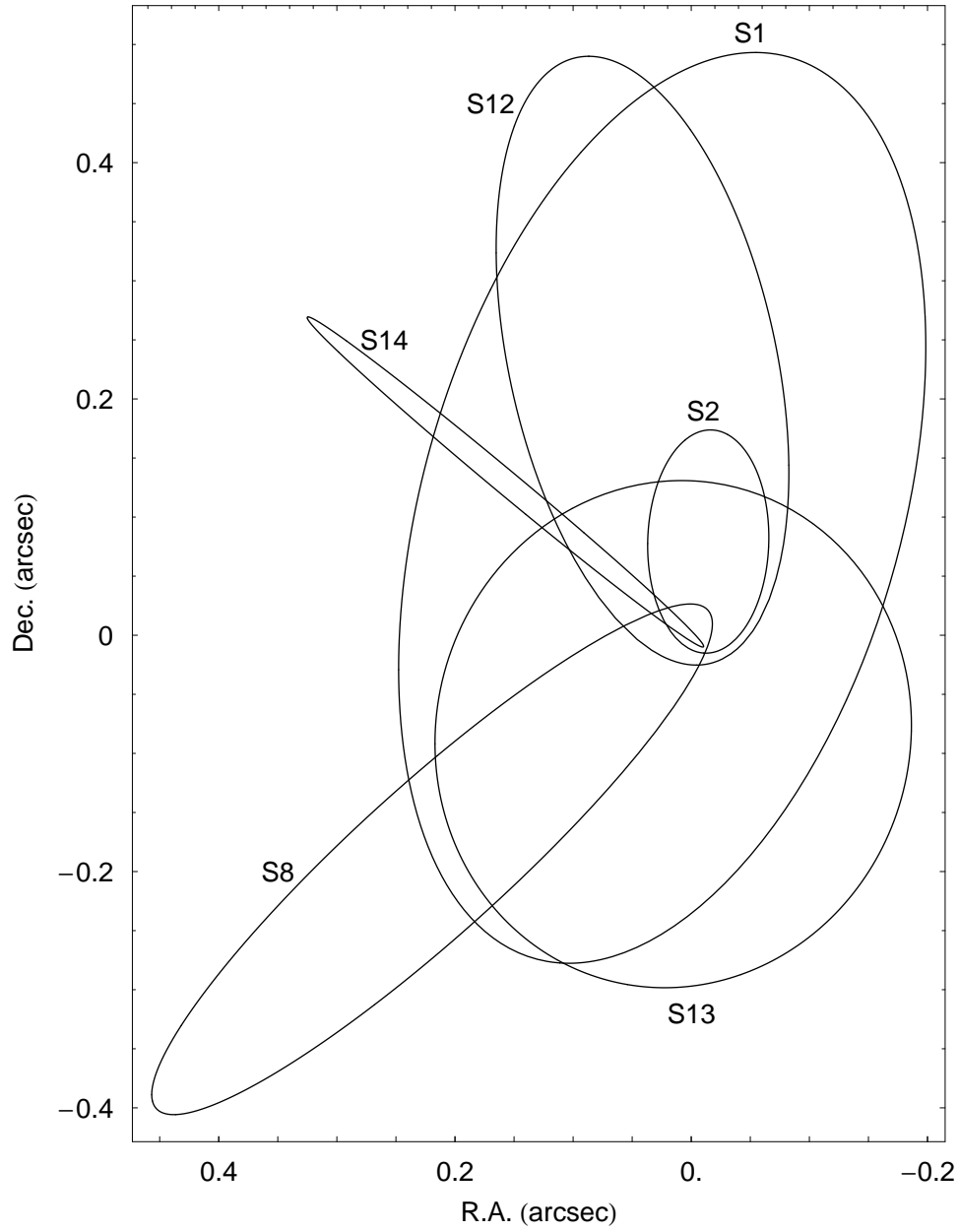


Fig. 3.— Orbits of the stars S2, S12, S14, S1, S8, S13 around Sgr A*, following Eisenhauer et al. (2005).

Among our stars, the minimum distance from the central black hole is reached by S14, which touches 110 AU, still 1545 times greater than R_{Sch} . Hence, we can safely consider, from the gravitational lensing point of view, both the observer and the source as being infinitely distant from the lens. The case of a source orbiting very close to the lens has been examined in the context of stellar black holes by Cunningham & Bardeen (1973).

In order to calculate the position and the brightness of the gravitational lensing images of our stars, we need to track their position with respect to the central black hole as a function of time. In particular, we need their distance D_{LS} and their position angle γ with respect to the optical axis. By simple geometry, we can relate them to the anomaly angle from the periaipse, denoted by ϕ

$$D_{LS} = \frac{a(1 - e^2)}{1 + e \cos \phi} \quad (17)$$

$$\gamma = \arccos[\sin(\phi + \omega) \sin i], \quad (18)$$

where a is the semimajor axis, e is the eccentricity, i is the inclination of the orbit and ω is the periaipse anomaly with respect to the ascending node. To find ϕ as a function of time, we can use angular momentum conservation (neglecting corrections by possible deviations of the mass distribution from spherically symmetry), which provides a differential equation for $\dot{\phi}$

$$\frac{[a(1 - e^2)]^{3/2}}{\sqrt{GM_{enc}}(1 + e \cos \phi)^2} \dot{\phi} = 1, \quad (19)$$

where M_{enc} is the mass enclosed in the orbit of the star we are considering, related to the orbital period P by

$$GM_{enc} = 4\pi^2 \frac{a^3}{P^2}. \quad (20)$$

Integrating and inverting equation (19), we can get ϕ as a function of time, exploiting the initial condition $\phi(T_0) = 0$, with T_0 given in Table 1.

4. Results

In this section we shall present the outcome of the gravitational lensing analysis for our six stars. We will show the light curves of the secondary, third and fourth order images, and the expected trajectory of the secondary image with respect to the central black hole. In the following, we shall discuss the results individually for each of them.

S2. – The spectral analysis of S2 reveals it as a main sequence star of $15 M_{\odot}$ of class O8 – B0 (Ghez et al. 2003; Eisenhauer et al. 2005). It is also famous as the star providing

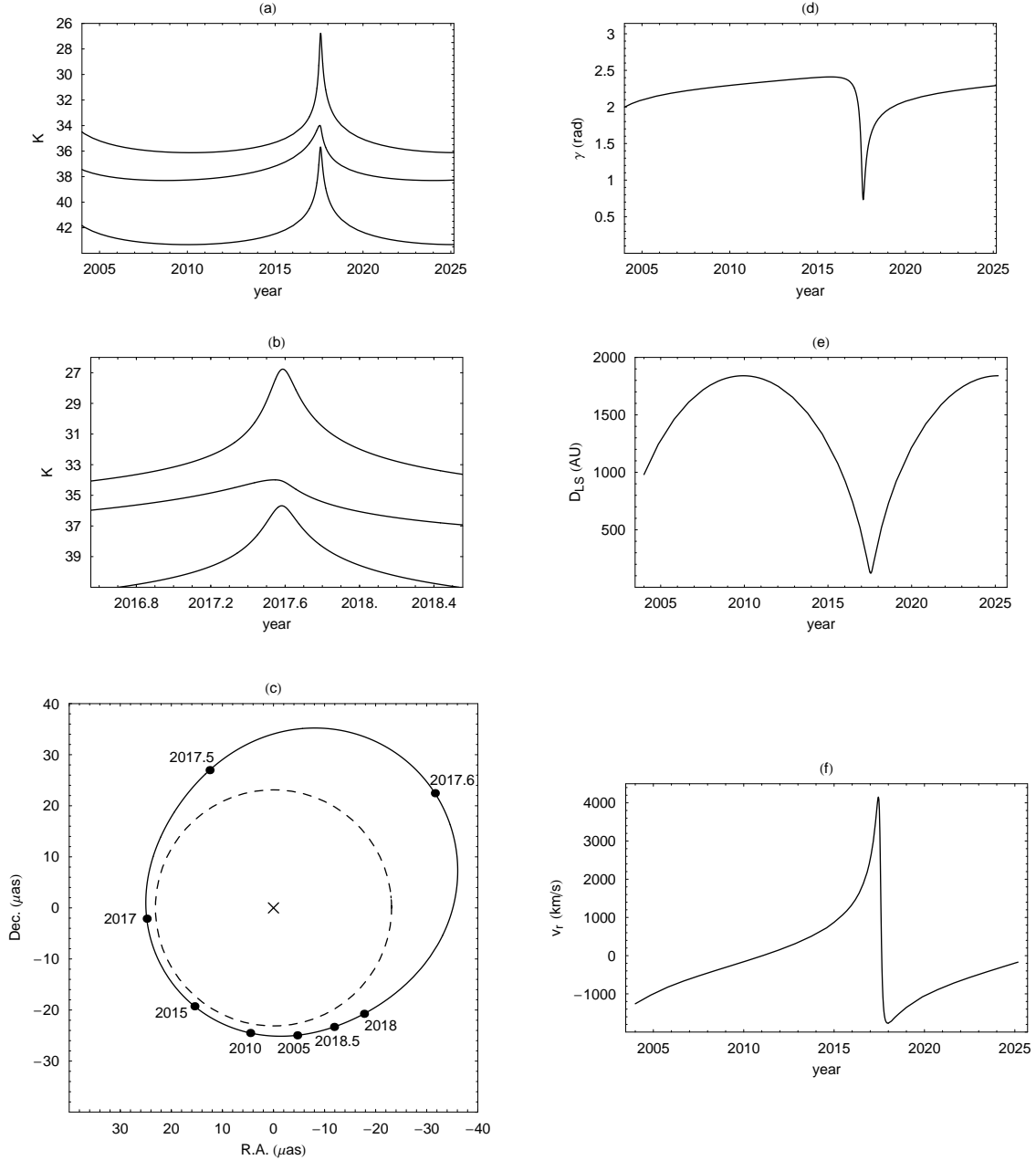


Fig. 4.— *S2*. – (a) Light curves for the gravitational lensing images of *S2*. From top to bottom, we have the secondary, the third order and fourth order images. (b) Details of the same light curves at the peak epoch. (c) Trajectory of the secondary image around the central black hole (marked by the cross in the middle). The dashed circle is its apparent horizon. (d) The angle γ , formed by the line connecting *S2* with the central black hole and the optical axis; (e) distance between *S2* and Sgr A*; (f) radial velocity of *S2*. All quantities are plotted as functions of time.

the best orbital constraint on the mass of the central black hole.

Figure 4a shows the apparent magnitudes in the K-band of its most important gravitational lensing images as functions of time, throughout the next orbital period. From top to bottom, we have the secondary image, the third order and the fourth order one. Their brightness changes very slowly during the whole orbital period, save for a sharp peak corresponding to the periaipse epoch, as it is evident from Figure 4e, which shows D_{LS} as a function of time. This is easily understood as a consequence of the D_{LS}^{-2} dependence in the magnification formula (14). In general, because of this dependence, we can say that highly eccentric orbits have more prominent peaks (once the inclination of the orbit has been fixed), since the minimum distance of the star from the black hole becomes smaller and smaller with respect to the maximum distance. Also the duration of the peak is determined by the eccentricity, in that the time the star spends to complete the passage at the periaipse is shorter for more eccentric orbits.

To be more quantitative, it is possible to show that for high eccentricities ($1 - e \ll 1$), the ratio between the duration of the peak and the orbital period scales as $1 - e$, while the ratio between the maximum and minimum brightness scales as $(1 - e)^{-2}$.

Figure 4b shows a detail of the peak epoch. We see that the new estimates for the orbital parameters of S2 bring the secondary image below $K=27$ in the middle of 2017. We recall that the previous estimates for the peak magnitude gave $K=30$ (De Paolis et al. 2003; Bozza & Mancini 2004) for the beginning of 2018. The third order image reaches $K=34$ at the same time, while the fourth order image has $K=36$.

In Figure 4c we report the trajectory of the secondary image around the central black hole, marked by a cross. The apparent event horizon is the circle of angular radius θ_m shown in dashed style. The trajectory of the secondary image is an ovoidal figure very close to the apparent event horizon for a large fraction of the orbital period. The distance of the image from the position of the central black hole is fixed by the lens equation (2). It basically depends on the angle γ , formed by the line joining the source to the lens with the optical axis. To see this correspondence in the specific case of S2, one can compare with Figure 4d, where γ is plotted as a function of time. We see that during the periaipse epoch, γ becomes smaller than $\pi/2$, which means that S2 is behind the black hole, the minimum value being 0.83 rad. At this epoch, the secondary image reaches the largest distance from the black hole. By contrast, during most of the period S2 is on the same side of the observer with respect to the black hole. During this period, the secondary image comes closer to the event horizon, since the photons require a larger deflection by the black hole in order to reach the observer.

The position angle of the secondary image around the black hole is always opposite to the position of the direct image, in the Schwarzschild black hole hypothesis. The third and fourth order images are formed very close to the apparent event horizon (their typical separation is a fraction of μas), so that in the scale of Figure 4c they would just be superposed on the dashed circle. Therefore, we omit them in all figures. For completeness, we have also included the plot of the radial velocity (Fig. 4f).

S12. – The results for this star are summarized in Figure 5. Here the maximal brightness is reached in C.E. 2050, when S12 will reach its minimum distance from Sgr A* again. At that time S12 will be in front of the black hole ($\gamma > \pi/2$), as can be seen from Figure 5d. Comparing the light curves for the images of S12 with those of S2, we find a very interesting difference. The magnification peaks are determined not only by the minimum D_{LS} , but also by the degree of alignment of the star with the optical axis. The peaks of the negative parity images (secondary and fourth order) are enhanced when γ is closer to 0, i.e., when the star lies behind the black hole. The third order image and the other positive parity images are maximally magnified when γ is closer to π , i.e., when the star lies in front of the black hole. Since S2 is behind the black hole at the periaapse, the secondary and fourth order images are strongly enhanced, while the third order image has only a quite small peak. The brightness of the fourth order image almost reaches that of the third order image. On the contrary, S12 is in front of the black hole at the periaapse, and the third order image is more enhanced than the secondary and the fourth order image. Its brightness almost reaches that of the secondary image. Moreover, since the minimum value of γ is reached just few months after the periaapse, the peaks of the secondary and of the fourth order images are broadened and "attracted" toward the time at which γ is minimal. The same happens to the third order image of S2, which is stretched toward earlier times, when γ is closer to π . A radical difference with respect to S2 also arises in the trajectory of the secondary image. Looking at Figure 5c, we see that the secondary image spends most of the time at larger distances from the black hole, since S12 is behind the black hole for most of its orbit (Fig. 5d). During the periaapse, S12 very quickly passes in front of the black hole and the secondary image grazes the apparent horizon making half of the tour in a very short time. This situation is the opposite of that of S2, which is in front of the black hole for most its orbit and behind it just at the periaapse. Another interesting thing to notice is that the secondary image of S12 does not move very far from the apparent horizon, since the orbit has a lower inclination and γ is bounded to a lower range around $\pi/2$.

S14. – This star represents the most interesting lensing candidate, since its orbit is almost edge-on ($i = 97.3$ deg), and its eccentricity brings it very close to the black hole. The best alignment and anti-alignment times are very close to the periaapse epoch and are responsible for two subpeaks, which are unresolved in Figure 6a, but clearly visible in Figure

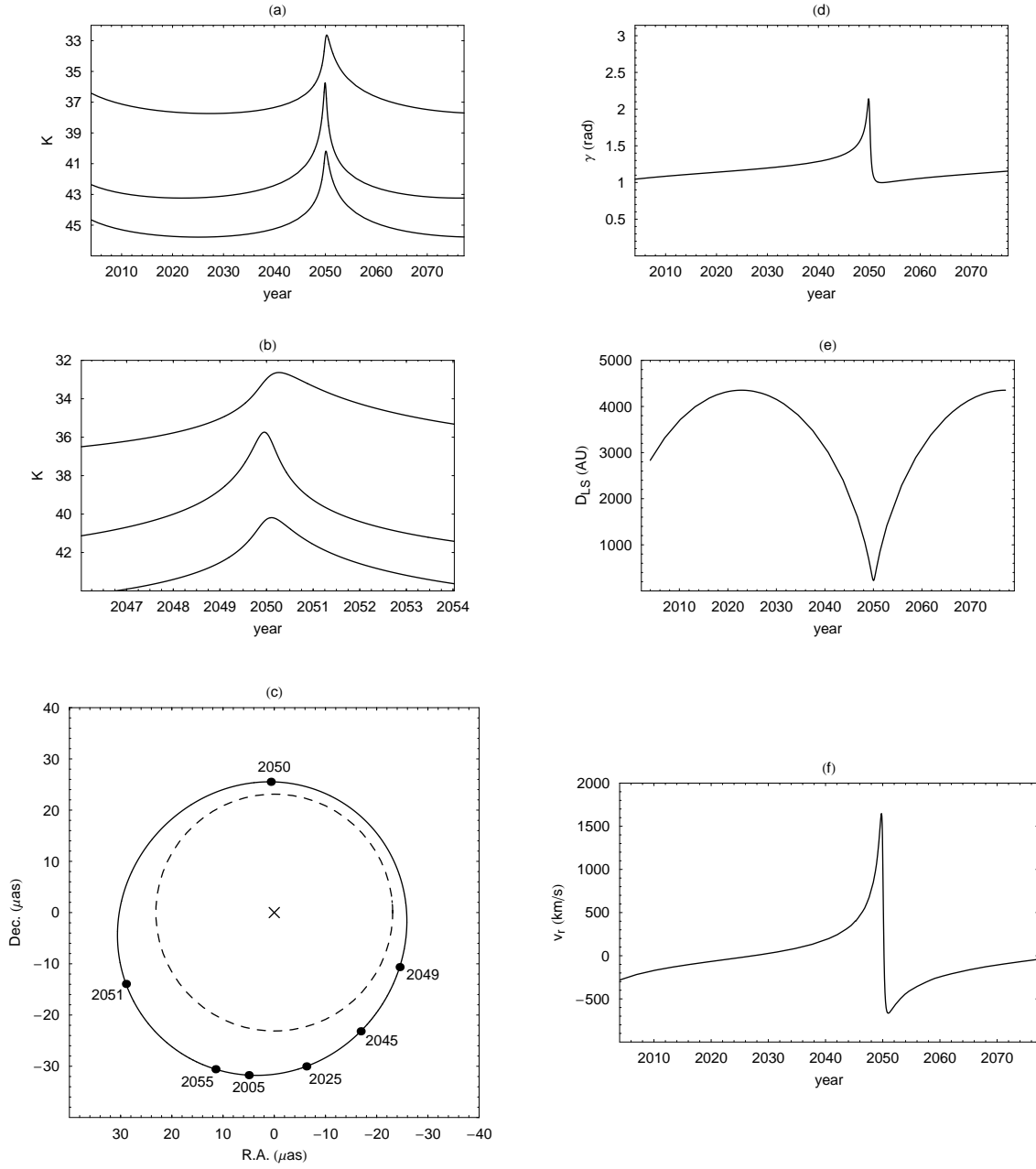


Fig. 5.— Results for S12. For the meaning of each panel, refer to the caption of Fig. 4.

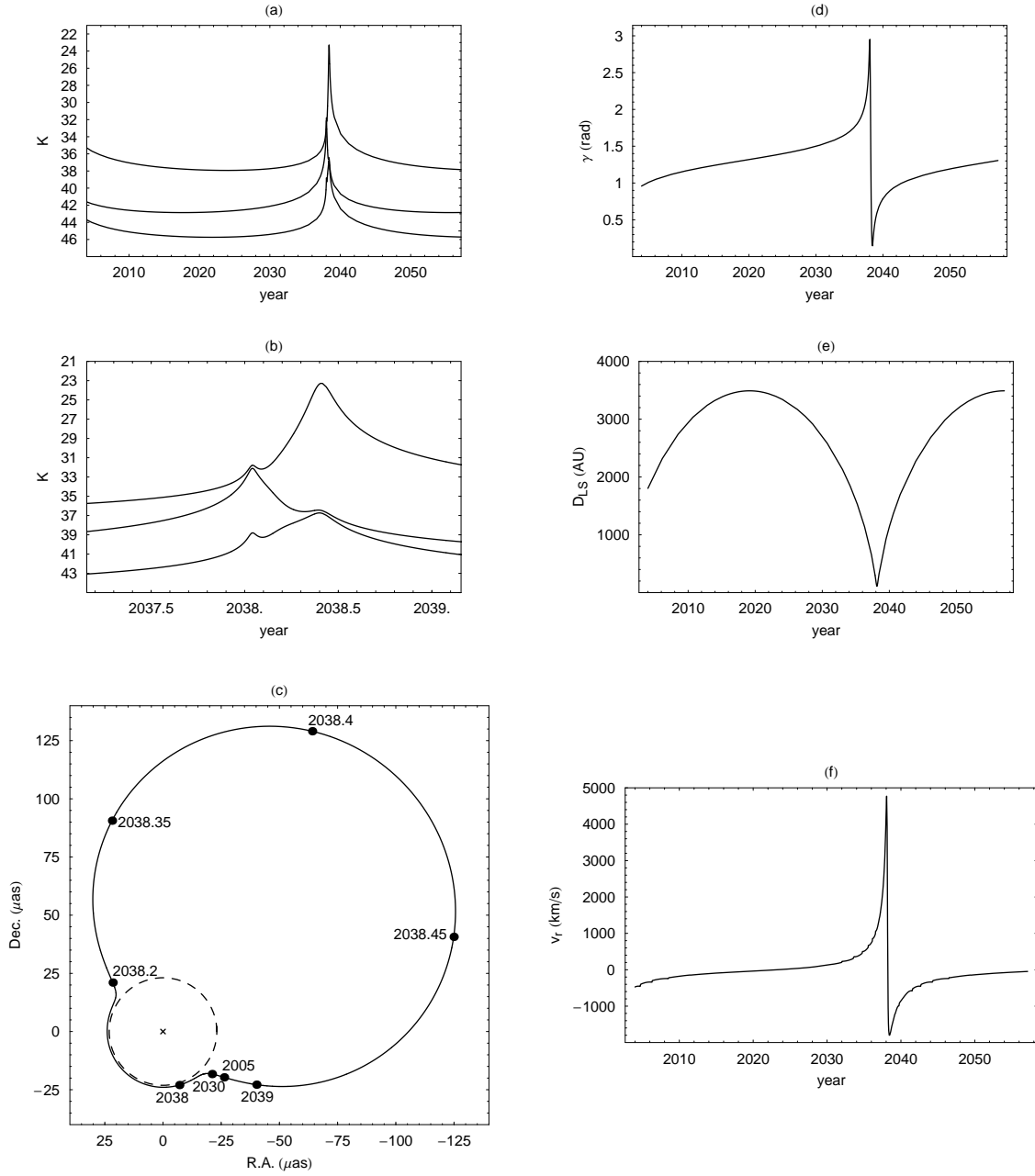


Fig. 6.— Results for S14. For the meaning of each panel, refer to the caption of Fig. 4.

6b, which zooms on the peak. The periaapse takes place while $\gamma \sim \pi/2$, so that this represents an intermediate case with respect to the former ones. First we have the anti-alignment peak, mostly enhancing the third order image, which reaches the brightness of the secondary image. Then we have the alignment peak, which mostly enhances the secondary and fourth order images. If the periaapse coincided with the best alignment or anti-alignment time, the corresponding peak would have been much more prominent than shown in Figure 6b.

What makes S14 particularly interesting is the high brightness attained by the secondary image. At the best alignment time the secondary image has $K=23$. This is because we are close to a weak field gravitational lensing situation as can also be seen by the analysis of Figure 6c. The trajectory of the secondary image is composed by two half rings: one grazing the apparent horizon when S14 is in front of the black hole and the other being the approximate weak field solution for the secondary image in a typical microlensing event. In fact, consider a source passing behind a point-lens along the line parameterized by

$$\vec{y} = (vt, b_0), \quad (21)$$

where v is the transverse velocity and b_0 is the microlensing impact parameter. Then the approximate solution for the secondary image in the case $b_0 \gg 1$ is

$$\vec{x} \simeq \frac{1}{b_0^2 + v^2 t^2} (-vt, -b_0), \quad (22)$$

which parameterizes a circle of radius $1/2b_0$ centered at $(0, -1/2b_0)$. This is exactly the big circle described by the secondary image in Figure 6c, apart from small distortions caused by the curvature of the orbit of S14.

The duration of the main peak is about one month and is determined by the velocity of S14 at the periaapse epoch. One may wonder whether the direct image is affected in a significant way by this almost weak field event. However, we find $\Delta\mu/\mu \sim 10^{-3}$ for the direct image, which makes the peak practically unobservable. The next brightness peak of the secondary image of S14 will occur in c.e. 2038, according to the current estimates of the orbital parameters, and the maximal angular distance from the apparent event horizon is about 0.125 mas. The perspectives for the observation of such event will be discussed in the next section.

The third order image reaches $K=32$, deserving particular attention, since the eventual observation of such image would be of striking importance for the physics of the gravitational field in the strong regime.

S1. – This star is characterized by a lower eccentricity, as clearly visualized in Figure 7e, where the range of values of D_{LS} is small, and in Figure 7f, where we see low radial velocities

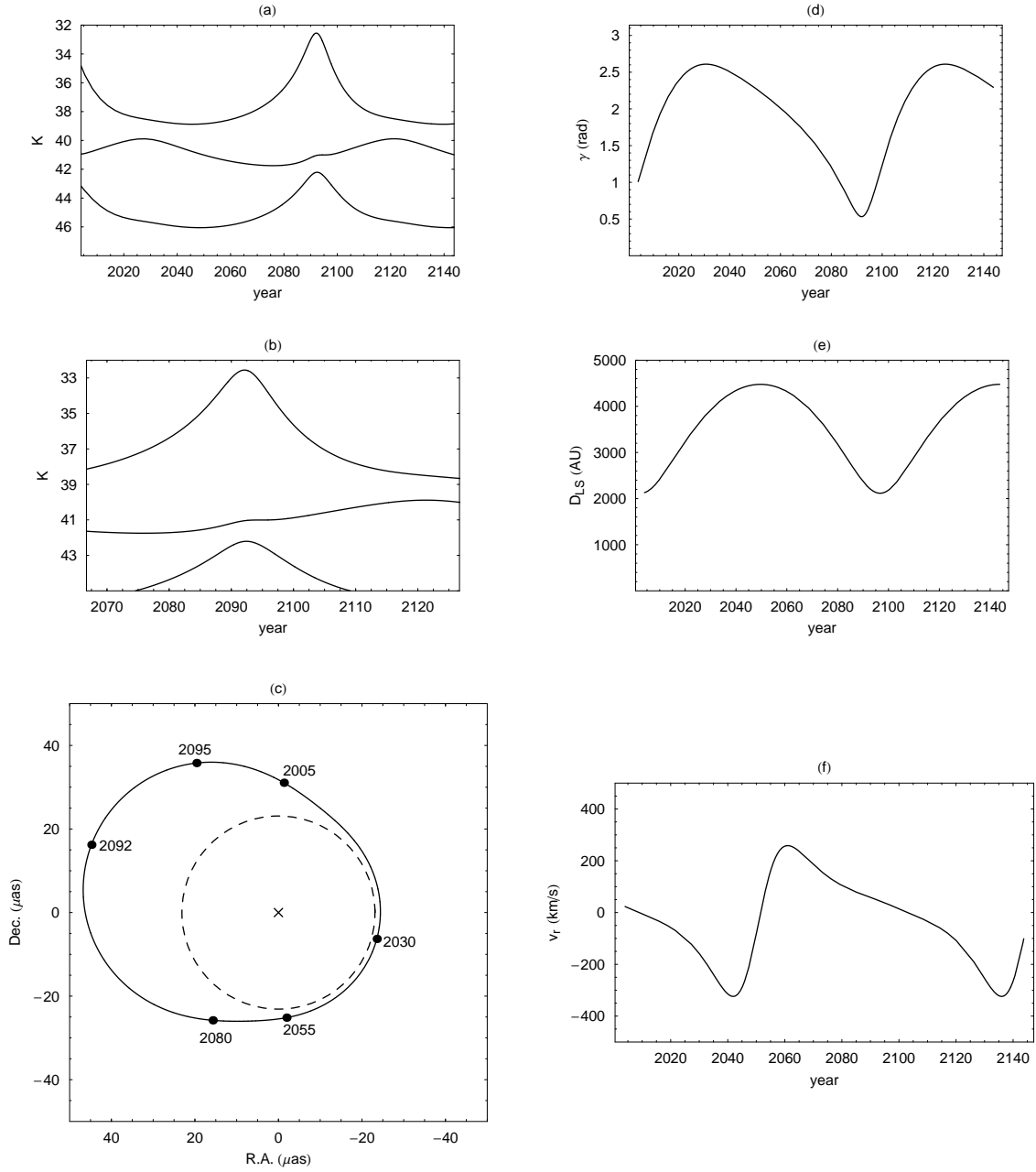


Fig. 7.— Results for the star S1. For the meaning of each panel, refer to the caption of Fig. 4.

compared to the other stars. It happens that the periaipse is in coincidence with the best alignment time, (see Fig. 7d), and in fact the peaks in the secondary and fourth order images are very enhanced, while the third order image has only a small modulation throughout the orbit (Fig. 7a). We also observe that the third order image has a small secondary peak at the best alignment time, which is formed in a way analogous to that discussed for S14. In any event, the secondary image will stay fainter than $K=32$ at the next peak, occurring only in c.E. 2091, so that this is a less interesting case for observations.

The trajectory of the secondary image (Fig. 7c) can be easily interpreted from the considerations given in the previous cases.

S8. – This star is known to have a high eccentricity (so high that, before the last data were released, it was still unclear whether the orbit was open or closed (Ghez et al. 2005)). According to Eisenhauer et al. (2005), the orbit is closed and it makes sense to discuss predictions for the next brightness peaks. Even though the periaipse distance is small, the inclination is not very high, so that we do not have the same favorable situation as S14. In c.E. 2054, the secondary image will "only" reach $K=28$. The periaipse lies between the best alignment and anti-alignment times, being a bit closer to the first configuration. Then the secondary and fourth order image peaks are a bit more prominent than the peak of the third order image, which also shows a very small deformation at the best alignment time.

S13. – For this star the uncertainty on the orientation of the orbital plane remains very large. So, our predictions can just give an indication, which will be updated when further measurements are available. In any case, the inclination of the orbital plane should be quite low and the images have a nearly constant low brightness, as shown in Figure 9a. The distance of the secondary image from the black hole is also nearly constant. Hence, this star also seem less promising as a candidate for gravitational lensing observations.

Table 2 summarizes the main characteristics of the gravitational lensing images for our six stars, allowing an immediate reading of all results.

5. Perspectives for observations

From our analysis, S14 emerges as the most interesting lensing candidate, because of its small minimum distance from the black hole and because of the high inclination of its orbit, which allows good alignments and anti-alignments with Sgr A*. The secondary image will reach $K=23$ at the next periaipse epoch, which will occur around c.E. 2038. The rapid motion of this image would help to distinguish it from background sources of similar brightness, while its distortion should also be an unambiguous sign of its gravitational lensing nature with

Parameter	S2	S12	S14	S1	S8	S13
a (arcsec)	0.1226 ± 0.0025	0.286 ± 0.012	0.225 ± 0.022	0.412 ± 0.024	0.329 ± 0.018	0.219 ± 0.058
P (yr) ...	15.24 ± 0.36	54.4 ± 3.5	38.0 ± 5.7	94.1 ± 9.0	67.2 ± 5.5	36 ± 15
e	0.8760 ± 0.0072	0.9020 ± 0.0047	0.9389 ± 0.0078	0.358 ± 0.036	0.927 ± 0.019	0.395 ± 0.032
T_0 (yr) ..	2002.315 ± 0.012	1995.628 ± 0.016	2000.156 ± 0.052	2002.6 ± 0.6	1987.71 ± 0.81	2006.1 ± 1.4
i (deg) ..	131.9 ± 1.3	32.8 ± 1.6	97.3 ± 2.2	120.5 ± 1.0	60.6 ± 5.3	11 ± 35
Ω (deg) ..	221.9 ± 1.3	233.3 ± 4.6	228.5 ± 1.7	341.5 ± 0.9	141.4 ± 1.9	100 ± 198
ω (deg) ..	62.6 ± 1.4	311.8 ± 3.6	344.7 ± 2.2	129.8 ± 4.7	159.2 ± 1.8	250 ± 161
K (mag)	13.9	15.5	15.7	14.7	14.5	15.8

Table 1: Orbital parameters of the six stars examined in the paper: a is the semimajor axis, P is the orbital period, e is the eccentricity, T_0 is the epoch of periaapse, i is the inclination of the normal of the orbit with respect to the line of sight, Ω is the position angle of the ascending node, ω is the periaapse anomaly with respect to the ascending node (data taken from Eisenhauer et al. 2005). K is the magnitude in the K-band, taken from Schödel et al. (2003).

	S2	S12	S14	S1	S8	S13
K_2 (mag)	26.8	32.6	23.3	32.6	27.6	36.2
T_2 (yr) ..	2017.59	2050.27	2038.41	2092.13	2054.7	2041.38
$\Delta\theta_2$ (μ as)	16	9.8	125	25	26	5.6
K_3 (mag)	34.0	35.7	32.1	39.9	34.8	39.9
T_3 (yr) ..	2017.54	2049.95	2038.04	2121.29	2055.2	2042.33
$\Delta\theta_3$ (μ as)	0.33	0.25	0.62	0.41	0.42	0.17
K_4 (mag)	35.7	40.2	36.7	42.2	37.3	43.7
T_4 (yr) ..	2017.58	2050.11	2038.4	2092.44	2054.74	2041.8
$\Delta\theta_4$ (μ as)	0.014	0.011	0.026	0.017	0.017	0.007

Table 2: Summary of the main features of the relativistic images of the six stars examined in this paper. K_i is the peak K-band magnitude for the i -th image; T_i is the time of the peak; $\Delta\theta_i = \theta_i - \theta_m$ is the maximal angular distance from the apparent event horizon.

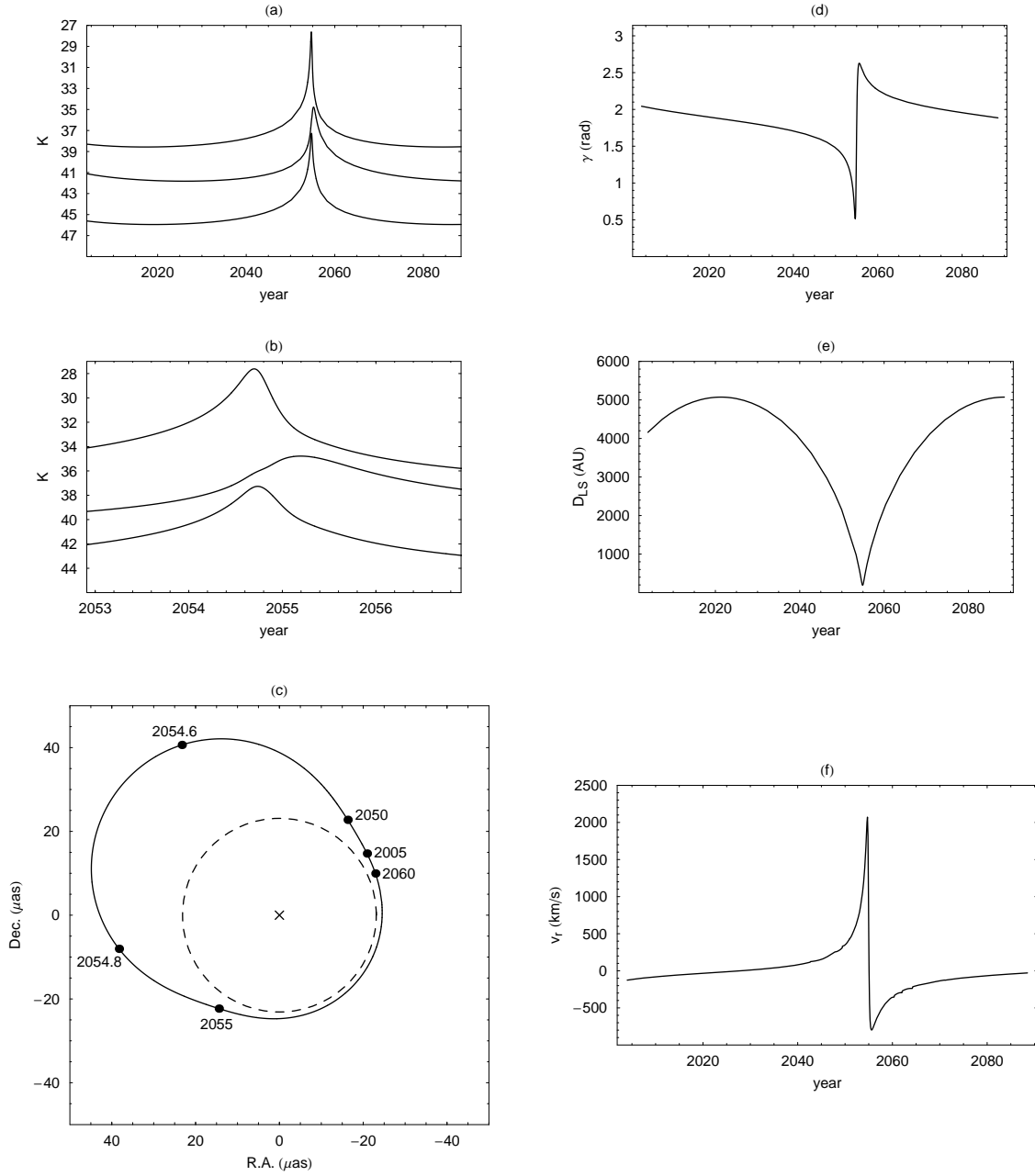


Fig. 8.— Results for S8. For the meaning of each panel, refer to the caption of Fig. 4.

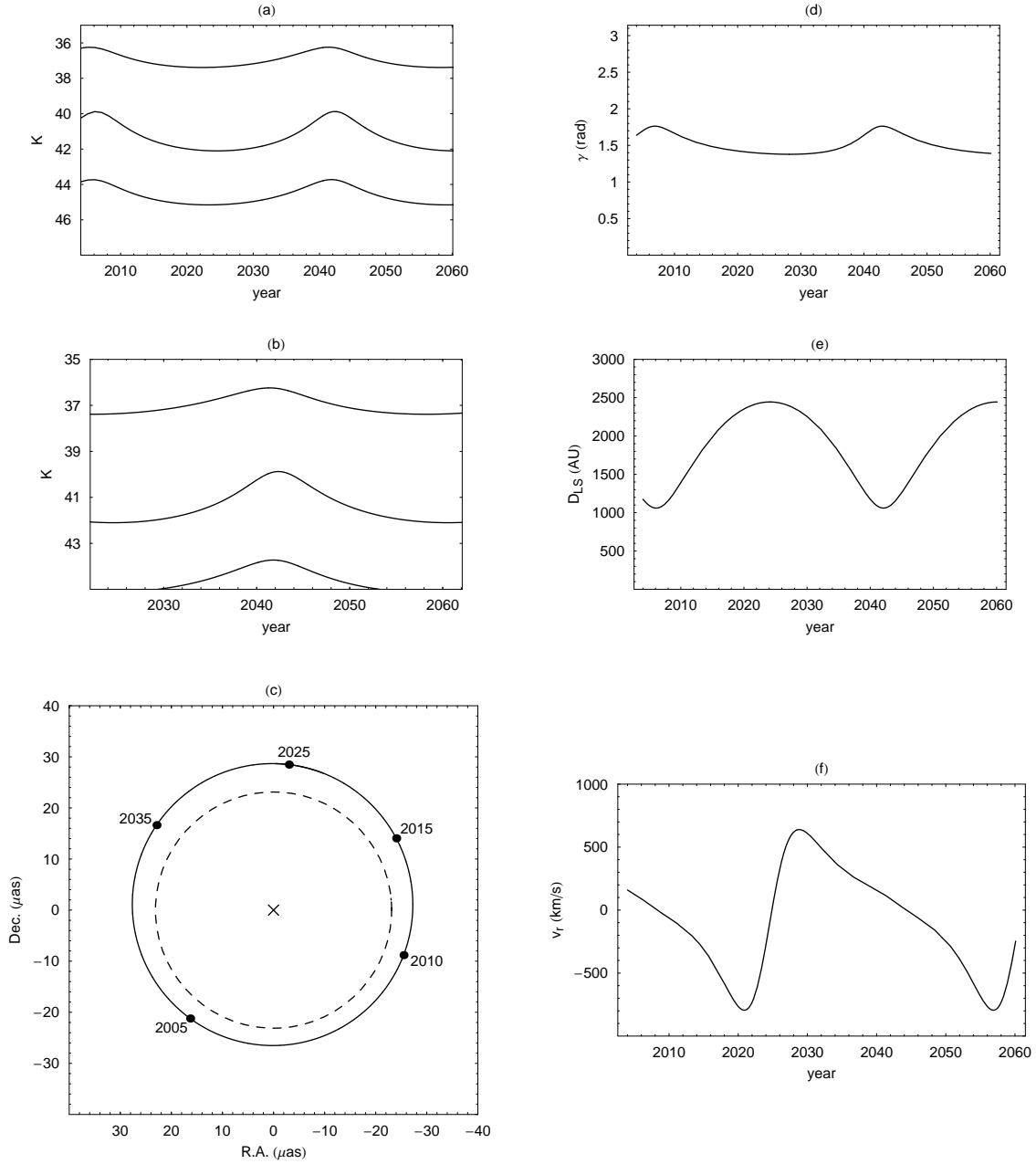


Fig. 9.— Results for S13. For the meaning of each panel, refer to the caption of Fig. 4.

respect to fast moving stars around Sgr A*. The theoretical baseline needed to resolve two sources of comparable brightness placed at an angular distance of $\theta = 0.12$ mas in the K-band, amounts to $\lambda/\theta = 3.8$ km. However, the apparent magnitude of Sgr A* is $K=18.8$ (Ghez et al. 2004; Genzel et al. 2003), which means that we have to distinguish a faint source from a 63 times brighter contaminant. This complication can be tackled by longer baselines and nulling interferometry techniques. Sgr A* is still unresolved in this band. One may be worried that if its infrared flux comes from a region of several Schwarzschild radii, then the secondary images of lensed stars would be merged within its diffuse infrared emission. However, current models explaining the rapid observed variability suggest that this emission takes place within $10 R_{Sch}$ from the central black hole (Yuan et al. 2004). In this case, the secondary image of S14 would come out of the infrared emission of Sgr A* and could be resolved, in principle, by interferometry facilities.

At the present time, the best resolution in the K-band is achieved by the Keck telescope and the VLT units, the latter reaching 75 mas without interferometry, thanks to active and adaptive optics. The VLT units can be combined to perform interferometry observations with an equivalent baseline of 200 m and a maximal angular resolution of 2.2 mas (<http://www.eso.org/projects/vlti>). A new interferometric instrument under construction is the Large Binocular Telescope (LBT), which will use two 8.4 m telescopes reaching an equivalent resolution of a 22 m telescope (<http://medusa.as.arizona.edu/lbto>).

New perspectives are opened by space telescopes. The Terrestrial Planet Finder (TPF) will be composed by four 3.5 m telescopes working in team. The design details are still under study; in particular, the four units may be mounted on the same structure or flying in formation several meters apart (<http://www.terrestrial-planet-finder.com>). A similar project is DARWIN, which will exploit six telescopes flying in formation with an equivalent aperture of 50 meters (<http://ast.star.rl.ac.uk/darwin>). These two missions are foreseen to launch around 2015 and are mainly aimed at exoplanet researches. The problem of resolving a faint planet from its mother-star, which is typically millions of times brighter, can be faced by the technique of nulling interferometry, which combines the signal from a number of different telescopes in such a way that the light from the central star is cancelled out, leaving the much fainter planet easier to see. Of course the situation of a faint gravitational lensing image close to Sgr A* has great analogies with that of exoplanets and the same techniques can be used. In order to achieve resolutions better than 0.1 mas, we need a baseline larger than several kilometers, which must be kept stable at a very high precision. A similar problem is faced by the LISA mission in the search for gravitational waves. In this mission, three spacecraft should fly in a triangular formation at relative distances of 5 million km (<http://lisa.nasa.gov>). Finally, the MAXIM mission will perform X-ray interferometry with a constellation of several spacecraft and a detector kept 450 km behind the mirrors

(<http://maxim.gsfc.nasa.gov>). To accomplish formation flying with high accuracy, these missions are planning to use a laser ranging system between spacecraft and microthrusters to offset drifts.

Given the present situation and all the technical advances that will soon be exploited in scientific researches, 0.1 mas resolution in the K-band and the detection of secondary gravitational lensing images around Sgr A* seem just the next step after the generation of telescopes currently under study. Hopefully, new instruments will be available before the next periaapse passage of S14 is in c.E. 2038, to catch its secondary image. For S2 and S8 the situation is more difficult, since the peak magnitude and the angular separations of the secondary images are lower, but the numbers do not rule out the possibility of observing them with reasonable future facilities.

As regards higher order images, S14 is still the best candidate. However, the peak magnitude of the third order image is $K=32.1$, and the separation from the apparent horizon is only $0.62 \mu\text{as}$. In order to see such a faint image so close to the event horizon we would need a complete imaging at very high resolution ($< 0.1 \mu\text{as}$) of Sgr A*. In the K-band this seems a very difficult task. The highest resolution ever reached is $18 \mu\text{as}$ in the mm band of the electromagnetic spectrum (Krichbaum et al. 2002). Higher resolution imaging seems to be possible at sub-mm wavelengths (Falcke et al. 1999), though no compact radio sources (suitable for gravitational lensing) are known around Sgr A*. Finally, MAXIM claims that a $0.1 \mu\text{as}$ resolution is achievable in the X-ray band. In this case, one should look for suitable X-ray sources around the Galactic center, which could be provided by a recently observed population of black holes within 1 pc from Sgr A* (Muno et al. 2004). Higher order images thus stand as a possible long-term target for future observations.

6. Discussion and Conclusions

It is really amazing that at present time it makes sense to discuss on gravitational lensing in strong fields by real physical objects. Indeed, the existence of a supermassive black hole at the center of our Galaxy with its rich stellar environment provides a unique laboratory for this research. However, this would not be enough without the great technical advances in high resolution observations of the last years, which allow us to speak about microarcsecond resolutions in sub-mm observations and possibly in higher frequency bands. The proper motion observations of stars surrounding Sgr A* are progressing daily, providing more and more precise estimates for the orbital parameters. In this work, we have analyzed six stars enjoying a good determination of their orbital parameters. Our aim has been to look for observable gravitational lensing effects on these stars by the black hole in Sgr A*. Our

investigation has considered the full set of gravitational lensing images, including weak field and relativistic ones, the latter being of striking importance for a deeper understanding of General Relativity, as they provide observational tests for gravitational theories in previously unprobed regimes. We have explicitly shown the light curves of the secondary, third order and fourth order images for our six stars. Moreover, we have shown the position in time of the secondary image w.r.t. the central black hole. We have given physical interpretations to our results, relating, in particular, the peaks to minima of D_{LS} and best alignment and anti-alignment times.

We want to stress that this work is just a first analysis, which is susceptible to be corrected by eventual upcoming estimates of the orbital parameters, enlarged to eventual new candidate stars, and generalized to different classes of black holes. The most physically motivated generalization of the Schwarzschild black hole is of course the Kerr solution. However, while in the Schwarzschild case the deflection angle can be still expressed analytically by equation (6), the treatment of gravitational lensing by Kerr black holes is done in a completely numerical way at the present time (Cunningham & Bardeen 1973; Viergutz 1993; Rauch & Blandford 1994). Moreover, the exact value of the spin of Sgr A* is still very uncertain and inferred by indirect deductions (Liu & Melia 2002; Aschenbach 2004). The deviations from the Schwarzschild predictions are bigger for higher order images, while they become very small in the weak field limit. This means that a high value of the spin would considerably alter the predictions for higher order images, but, for example, the peak of the secondary image of S14 would be affected in a negligible way. So, for a first analysis, Schwarzschild lensing is basically sufficient to understand the highlights of the lensing scenario and the order of magnitude of the observables. Kerr lensing comes as a second step refinement.

Another topic that deserves some discussion concerns the uncertainties in our predictions coming from the present uncertainties in the estimates of the orbital parameters. The first thing to notice is that all these stars have been observed during their periaapse epochs. We can thus be confident that even if the semimajor axis and the eccentricity are affected by large errors, the periaapse distance is well determined by direct observations. Since the inclinations are also relatively well determined, we can conclude that the magnitudes of the peaks cannot be very different from the ones that we have calculated using the best-fit values of the orbital parameters. By contrast, the precise timing of the peaks is strictly related to the accuracy of the orbital period estimate. This can be established only with a good sampling on the whole orbit which requires more systematic observations in the future. As an example, given the present uncertainties, the brightness peak of the images of S14 could be displaced few years later or before the date that we have indicated using the best-fit value.

Finally, with the progress of the observation techniques, it is inevitable that new stars will be discovered around Sgr A* and followed during their orbits. If new stars are discovered closer and closer to Sgr A*, then the thin lens approximation cannot be used any longer. In that case, the analysis should proceed in the way indicated by Cunningham & Bardeen (1973). All these considerations make us confident that even better candidates than S14 may be found in the future to open the era of gravitational lensing by strong fields.

We thank Gaetano Scarpetta for useful comments on the manuscript. We also thank the referee for many suggestions which have helped us to improve our paper considerably.

REFERENCES

- Alexander, T. 2001, *ApJ*, 553, L149
- Alexander, T., & Loeb, A. 2001, *ApJ*, 551, 223
- Alexander, T., & Sternberg, A. 1999, *ApJ*, 520, 137
- Aschenbach, B. 2004, astro-ph/0406545
- Bozza, V. 2002, *Phys. Rev. D*, 66, 103001
- Bozza, V. 2003, *Phys. Rev. D*, 67, 103006
- Bozza, V., Capozziello, S., Iovane, G. & Scarpetta, G. 2001, *Gen. Rel. and Grav.*, 33, 1535
- Bozza, V. & Mancini, L. 2004, *ApJ*, 611, 1045
- Chanamé, J., Gould, A., & Miralda-Escudé, J. 2001, *ApJ*, 563, 793
- Cunningham, C.T., & Bardeen, J.M. 1973, *ApJ*, 183, 237
- Darwin, C. 1959, *Proc. of the Royal Soc. of London*, 249, 180
- De Paolis, F., Geralico, A., Ingrosso, G. & Nucita, A.A. 2003, *A&A*, 409, 809
- Eckart, A., & Genzel, R. 1997, *MNRAS*, 284, 576
- Eckart, A., Genzel, R., Ott, T., & Schödel, R. 2002, *MNRAS*, 331, 917
- Eiroa, E.F. & Torres, D.F. 2004, *Phys. Rev. D*, 69, 063004

- Eisenhauer, F., Genzel, R., Alexander, T., et al. 2005, astro-ph/0502129
- Falcke, H., Melia, F., & Agol, E. 1999, ApJ, 528, L13
- Genzel, R., Thatte, N., Krabbe, A., et al. 1996, ApJ, 472, 153
- Genzel, R., Schödel, R., Ott, T., et al. 2003, Nature, 425, 934
- Ghez, A.M., Klein, B.L., Morris, M., & Becklin, E.E. 1998, ApJ, 509, 678
- Ghez, A.M., Duchêne, G., Matthews, K., et al. 2003, ApJ, 586, L127
- Ghez, A.M., Wright, S. A., Matthews, K., et al. 2004, ApJ, 601, L159
- Ghez, A.M., Salim, S., Hornstein, et al. 2005, ApJ, 620, 744
- Jaroszyński, M. 1998, Acta Astron., 48, 413
- Krichbaum, T.P., Graham, D.A., Alef, W., et al. 2002, Proc. 6th European VLBI Network Symposium, Bonn, Germany, astro-ph/0207022
- Liu, S., & Melia, F. 2002, ApJ, 573, L23.
- Melia, F., & Falcke, H. 2001, ARA&A, 39, 309
- Muno, M.P., Pfahl, E., Baganoff, F.K., et al. 2004, astro-ph/0412492
- Nusser, A., & Broadhurst, T. 2004, astro-ph/0407220
- Ohanian, H. 1987, Amer. Jour. Phys., 55, 428
- Petters, A.O. 2003, MNRAS, 338, 457
- Rauch, K.P., & Blandford, R.D. 1994, ApJ, 421, 46
- Reid, M.J. 1993, ARA&A, 31, 345
- Schödel, R., Ott, T., Genzel, R., et al. 2002, Nature, 419, 694
- Schödel, R., Ott, T., Genzel, R., et al. 2003, ApJ, 596, 1015
- Viergutz, S.U. 1993, A&A, 272, 355
- Virbhadra, K.S., & Ellis, G.F.R. 2000, Phys. Rev. D, 62, 084003
- Wardle, M., & Yusuf-Zadeh, F. 1992, ApJ, 387, L65

Yuan, F., Quataert, E., & Narayan, R. 2004, ApJ, 606, 894